Dalton Transactions

PAPER

View Article Online
View Journal

Cite this: DOI: 10.1039/c8dt04634d

Coordination geometry-induced optical imaging of L-cysteine in cancer cells using imidazopyridine-based copper(II) complexes†

Selvarasu Priyanga,[a] Themmila Khamrang,[b] Marappan Velusamy,[b] Sellamuthu Karthi,[c] Balasubramaniem Ashokkumar[c] and Ramasamy Mayilmurugan*[a]

Overexpression of cysteine cathepsins proteases has been documented in a wide variety of cancers, and enhances the L-cysteine concentration in tumor cells. We report the synthesis and characterization of copper(II) complexes $[Cu(L1)_2(H_2O)](SO_3CF_3)_2$, **1**, L1 = 3-phenyl-1-(pyridin-2-yl)imidazo[1,5-*a*]pyridine, $[Cu(L2)_2(SO_3CF_3)]SO_3CF_3$, **2**, L2 = 3-(4-methoxyphenyl)-1-pyridin-2-yl-imidazo[1,5-*a*]pyridine, $[Cu(L3)_2(H_2O)](SO_3CF_3)_2$, **3**, L3 = 3-(3,4-dimethoxy-phenyl)-1-pyridin-2-yl-imidazo[1,5-*a*]pyridine and $[Cu(L4)_2(H_2O)](SO_3CF_3)_2$, **4**, L4 = dimethyl-[4-(1-pyridin-2-yl-imidazo[1,5-*a*]pyridin-3-yl)phenyl]amine as 'turn-on' optical imaging probes for L-cysteine in cancer cells. The molecular structure of complexes adopted distorted trigonal pyramidal geometry (τ, 0.68–0.87). Cu–N_{py} bonds (1.964–1.989 Å) were shorter than Cu–N_{imi} bonds (2.024–2.074 Å) for all complexes. Geometrical distortion was strongly revealed in EPR spectra, showing $g_{\|}$ (2.26–2.28) and $A_{\|}$ values (139–163 × 10^{-4} cm^{-1}) at 70 K. The d–d transitions appeared around 680–741 and 882–932 nm in HEPES, which supported the existence of five-coordinate geometry in solution. The Cu(II)/Cu(I) redox potential of **1** (0.221 V *vs.* NHE) was almost identical to that of **2** and **3** but lower than that of **4** (0.525 V *vs.* NHE) in HEPES buffer. The complexes were almost non-emissive in nature, but became emissive by the interaction of L-cysteine in 100% HEPES at pH 7.34 *via* reduction of Cu(II) to Cu(I). Among the probes, probe **2** showed selective and efficient turn-on fluorescence behavior towards L-cysteine over natural amino acids with a limit of detection of 9.9 × 10^{-8} M and binding constant of 2.3 × 10^5 M^{-1}. The selectivity of **2** may have originated from a nearly perfect trigonal plane adopted around a copper(II) center (~120.70°), which required minimum structural change during the reduction of Cu(II) to Cu(I) while imaging Cys. The other complexes, with their distorted trigonal planes, required more reorganizational energy, which resulted in poor selectivity. Probe **2** was employed for optical imaging of L-cysteine in HeLa cells and macrophages. It exhibited brighter fluorescent images by visualizing Cys at pH 7.34 and 37 °C. It showed relatively less toxicity for these cell lines as ascertained by the MTT assay.

Received 22nd November 2018,
Accepted 21st December 2018

DOI: 10.1039/c8dt04634d

rsc.li/dalton

Introduction

Biomolecules containing a thiol group such as L-cysteine (Cys), homocysteine (Hcy) and glutathione (GSH) have crucial roles in cellular function, including proliferation, antioxidant defense, signaling and maintaining redox homeostasis.[1] In particular, Cys has a pivotal role as an intracellular redox buffer that influences detoxification and critical metabolic functions; it is also a potential neurotoxin, a biomarker for various medical diagnoses and active-site protein in several metalloenzymes in body fluids.[2–5] Thus, a disproportionate level of Cys causes various adverse effects in human metabolism.[6–11] Specifically, protease enzymes known as "cysteine cathepsins" are located in the intracellular region, and are involved in protein degradation and processing in normal cell formation.[12] In tumor-cell formation, they are translocated to the cell surface and facilitate degradation of the extracellular matrix (ECM), which produces an abnormal amount of Cys by breaking disulfur linkages. The over-expression of cysteine cathepsins has been reported in a wide variety of cancers.[13] Hence, it is essential to study the pathway

[a]*Bioinorganic Chemistry Laboratory/Physical Chemistry, School of Chemistry, Madurai Kamaraj University, Madurai, 625021, India.*
E-mail: mayilmurugan.chem@mkuniversity.org
[b]*Department of Chemistry, North-Eastern Hill University, Shillong, 793022, India*
[c]*School of Biotechnology, Madurai Kamaraj University, Madurai, 625 021, India*

† Electronic supplementary information (ESI) available. CCDC 1833674–1833677. For ESI and crystallographic data in CIF or other electronic format see DOI: 10.1039/c8dt04634d

and activity of Cys to understand the key biological roles of cysteine cathepsins in the formation and proliferation of tumor cells. In addition, detection and imaging of thiol-containing molecules in cancer biology is very important to ensure early diagnosis and treatment of disease.

Some scholars have detected thiol-containing biomolecules that mostly utilize biologically unviable metals such as Ir, Cd, Hg and Ru.[14,15] Boron dipyrromethane (BODIPY), cyanine and coumarin fluorescent units have been reported as chemodosimetric sensors for the detection of thiol-containing compounds (Cys, Hcy, GSH) without selectivity or with poor selectivity.[16–22] Recently, Cu(II)-based probes have received much attention as 'optical probes' for imaging smaller metabolites and other biochemical reactions produced during the formation and proliferation of tumor cells.[24] As well explored in the literature, it is challenging to generate Cu^{II}–thiolate bonds due to the thermodynamically favorable redox reaction ($2RS^- + 2Cu^{II} \rightarrow RS\text{-}SR + 2Cu^{I}$).[25] In general, copper(II) is reduced by thiols and subsequently coordinated to cuprous ions for generation of Cu(I)–thiol complexes.[26] Only a few copper(II) complexes containing anthracene, coumarin, fluorescein, and zwitterionic bipyridine derivatives have been reported for the detection of thiols (Cys, Hcy, GSH) and histidine with poor selectivity, which were studied without any chemical-biology perspective.[23]

Very recently, we developed copper(II)-probes based on terpyridine and pyridine-bis-benzimidazole ligands for imaging of pre-incubated Cys in cancer cells, which showed excellent selectivity and limit of detection.[11,27] The Cys-probing mechanism is proposed to operate *via* reduction of copper(II) centers into copper(I) followed by displacement, which leads to regeneration of the fluorescent intensity of the original ligand at brighter visible-light emission regions. The preferable tetrahedral coordination geometry of copper(I) cannot be adopted by rigid terpyridine and pyridine-bis-benzimidazole ligand systems.[11,27]

In this report, we designed and synthesized new copper(II) complexes of bidentate imidazopyridine-based ligands and characterized them as optical probes for imaging of L-cysteine *via* a 'turn on' fluorescence mechanism. These ligands are expected to provide the required geometrical plasticity for the coordination of Cu(II) and Cu(I) ions. The ligand architecture was modified by substituting methoxy and $-NMe_2$ groups, and we expected to tune the structural properties and imaging mechanism. The *p*-substituted methoxy probe exhibited selective and efficient turn-on fluorescence behavior on interaction with Cys, and imaged Cys in cancer cells *via* reduction of copper(II) to copper(I) without ligand displacement. The probing mechanism was established by electronic spectral, redox and density functional theory (DFT) studies and live cell imaging by laser scanning fluorescence microscopy.

Results and discussion

Synthesis and characterization

The phenyl-substituted imidazopyridine-based ligands 3-phenyl-1-pyridin-2-yl-imidazo[1,5-*a*]pyridine (L1), 3-(4-methoxyphenyl)-1-pyridin-2-yl-imidazo[1,5-*a*]pyridine (L2), 3-(3,4-dimethoxy-phenyl)-1-pyridin-2-yl-imidazo[1,5-*a*]pyridine (L3) and dimethyl-[4-(1-pyridin-2-yl-imidazo[1,5-*a*]pyridin-3-yl) phenyl]amine (L4) were synthesized according to a methodology published previously with slight modifications (Scheme 1).[28] The reaction of substituted benzaldehyde with di-pyridin-2-yl-methanone in the presence of NH_4OAc and acetic acid yielded the respective ligands, which were characterized by nuclear magnetic resonance (NMR) spectroscopy. Copper(II) complexes were isolated as green solids by the reaction of one equivalent of $Cu(SO_3CF_3)_2$ with two equivalents of the corresponding ligands in acetonitrile at room temperature. The formation of the complexes was confirmed by high-resolution-mass spectrometry (HR-MS) (Fig. S1–S4†) and they were formulated as $[Cu(L1)_2(H_2O)](SO_3CF_3)_2$ **1**, $[Cu(L2)_2(SO_3CF_3)]SO_3CF_3$ **2**, $[Cu(L3)_2(H_2O)](SO_3CF_3)_2$ **3** and $[Cu(L4)_2(H_2O)](SO_3CF_3)_2$ **4**. The formulations were further supported by single-crystal X-ray structures. The suitable single crystals for X-ray diffraction were grown in acetonitrile by slow evaporation and diffusion methods.

Molecular structure of copper(II) complexes

The single-crystal X-ray structures of **1–4** are shown in Fig. 1 and their selected bond lengths, bond angles are summarized in Table 1. The complexes **1–3** were crystallized in a triclinic system with a space group of $P\bar{1}$, but the complex **4** was crystallized in a monoclinic system with a space group of $C2/c$. The molecular structure of **1–4** exhibited a distorted trigonal–bipyramidal coordination geometry as predicted by the Addison structural index τ, 0.68–0.87 [$\tau = (\beta - \alpha)/60$; for perfect square pyramidal and trigonal–pyramidal geometries, τ = 0 and 1, respectively].[29] The distorted trigonal bipyramidal geometry of copper(II) centers were constituted by the coordination of four nitrogens of the ligand units and one oxygen of water or triflate anion molecules. The complex **2** exhibited a higher τ value, 0.87, than that of **3** (τ, 0.75), which was lowered further to 0.68 for **1** and **4**. The electron-releasing *p*-methoxy substituent on the phenyl rings of **2** enabled exhibition of a higher τ value and adoption of more trigonal–bipyramidal coordination geometry (or less square pyramidal). In fact, N2, N5 and O1 donors constituted nearly a perfect trigonal plane around copper(II) centers, as evidenced by bond angles of 120.70° for N2–Cu–O1; 119.21° for N2–Cu–N5, and 120.06° for N5–Cu–O1. These bond angles deviated completely from 120° for **3** (111.3,

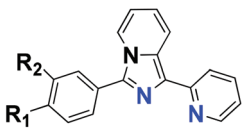

L1, R, R_2 = H
L2, R_1= -OCH_3, R_2 = H
L3, R_1, R_2 = -OCH_3,
L4, R_1= -$N(CH_3)_2$, R_2 = H

Scheme 1 Structure of ligands L1–L4.

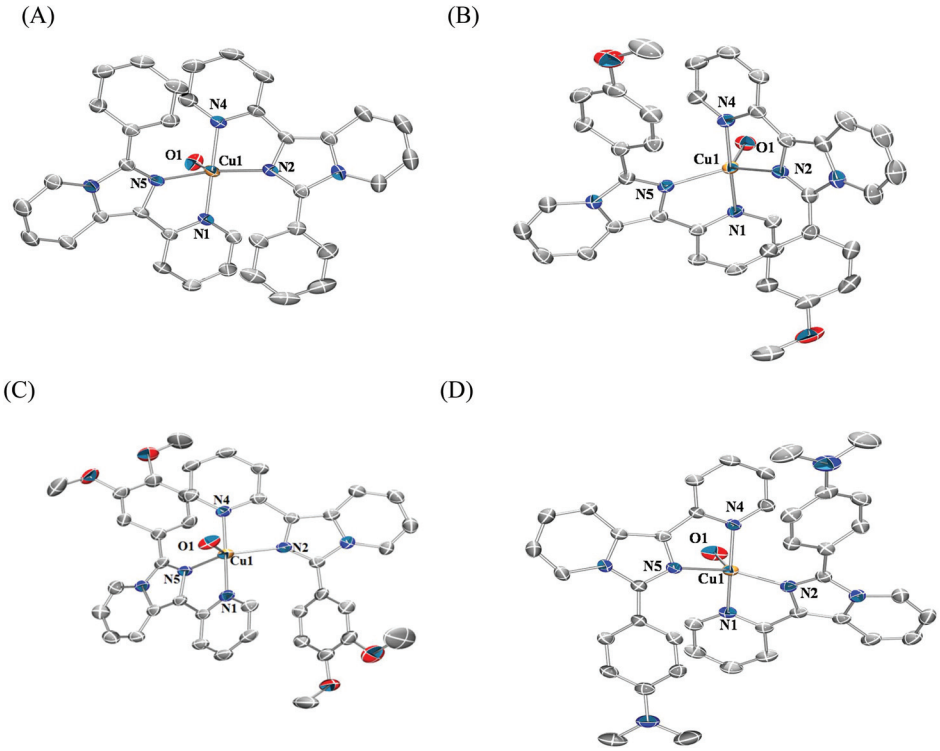

Fig. 1 Molecular structure of $[Cu(L1)_2(H_2O)](SO_3CF_3)_2$ **1** (A), $[Cu(L2)_2(SO_3CF_3)]$-(SO_3CF_3) **2** (B), $[Cu(L3)_2(H_2O)](SO_3CF_3)_2$ **3** (C) and $[Cu(L4)_2(H_2O)](SO_3CF_3)_2$ **4** (D). Thermal ellipsoids are drawn at the 40% probability level. Hydrogen atoms and $SO_3CF_3^-$ ions have been omitted for clarity.

Table 1 Selected bond lengths[a] [Å] and bond angles[a] [°] for **1–4**

	1	2	3	4
τ-Value	0.68	0.87	0.75	0.68
Cu(1)–N(1)	1.978(3)	1.964(3)	1.989(4)	1.982(3)
Cu(1)–N(4)	1.985(3)	1.980(3)	1.980(4)	1.976(3)
Cu(1)–N(2)	2.053(3)	2.050(3)	2.043(4)	2.024(3)
Cu(1)–N(5)	2.074(3)	2.048(3)	2.049(4)	2.054(3)
Cu(1)–O(1)	2.093(3)	2.174(3)	2.196(4)	2.167(3)
N(1)–Cu(1)–N(4)	175.28(12)	173.11(13)	173.58(17)	170.43(13)
N(1)–Cu(1)–N(2)	81.15(11)	81.12(13)	81.65(16)	81.43(14)
N(4)–Cu(1)–N(2)	100.88(11)	103.10(12)	99.94(16)	102.08(14)
N(1)–Cu(1)–N(5)	101.61(11)	101.51(12)	103.09(16)	102.98(13)
N(4)–Cu(1)–N(5)	81.30(10)	81.31(12)	80.90(17)	81.76(13)
N(2)–Cu(1)–N(5)	117.67(11)	119.21(12)	128.12(16)	129.61(13)
N(1)–Cu(1)–O(1)	87.49(11)	85.72(12)	86.86(17)	85.25(13)
N(4)–Cu(1)–O(1)	88.06(11)	87.43(12)	86.77(17)	85.50(13)
N(2)–Cu(1)–O(1)	133.95(11)	120.70(12)	111.3(2)	125.66(15)
N(5)–Cu(1)–O(1)	108.30(11)	120.06(12)	120.5(2)	104.70(15)

[a] Standard deviation in parenthesis; [$\tau = (\beta - \alpha)/60$; β(N1–Cu1–N4) = 175.28° and α(N2–Cu1–O1) = 133.95° for **1**. β(N1–Cu1–N4) = 173.11° and α(N2–Cu1–O1) = 120.70° for **2**. β(N1–Cu1–N4) = 173.64° and α(N2–Cu1–N5) = 128.11° for **3**. β(N1–Cu1–N4) = 170.44° and α(N2–Cu1–N5) = 129.62° for **4**; where by, for perfect square pyramidal and trigonal–bipyramidal geometries, τ = 0 and 1, respectively.

128.12, 120.5°) due to additional electron-releasing methoxy groups at the *meta*-position, and resulted in significant distortion in the trigonal plane as compared with **2**. Conversely, the more electron-releasing –NMe_2 group in **4** offered more distortion in the trigonal plane (N2–Cu–O1, 125.66; N2–Cu–N5, 129.6; N5–Cu–O1, 104.70°) and exhibited less trigonal–bipyramidal coordination geometry than that of **2** and **3**. These data clearly indicated that *p*-methoxy substituents on phenyl rings enforced a nearly perfect trigonal plane and that additional *m*-methoxy groups offered steric influence to deviate from the trigonal plane around copper(II) centers. The bond angles N1–Cu1–N4 (170.44–175.28°) of **1–4** deviated from 180°, indicating a distortion in the axial coordination. The $Cu–O_{water}$ bond distance of **1** (2.093 Å) was slightly shorter than those of **3** (2.196 Å), **4** (2.161 Å) and the $Cu–O_{triflate}$ bond of **2** (2.174 Å. The $Cu–N_{py}$ bonds (1.964–1.989 Å) of the complexes were shorter than the $Cu–N_{imi}$ bonds (2.024–2.074 Å). The strong overlapping of the p-orbital of pyridine nitrogen and d-orbital of the Cu(II) center led to shorter Cu–N bonds than those of imidazole nitrogen atoms. However, these Cu–N bond distances were longer than those of our previously reported square pyramidal complexes of terpyridine (1.970–2.069 Å)[11] and pyridine-bis-benzimidazole (1.958–2.000 Å) ligands.[27]

Electronic spectral studies

The electron paramagnetic resonance (EPR) spectra of the copper(II) complexes **1–4** were recorded in a methanol/DMF mixture at 70 K and found to be axial. The EPR spectra were simulated and their Hamiltonian parameters calculated, which were almost similar to that of the experimental data (Fig. S5,† Table 2). The hyperfine features resolved in the parallel ($g_{\|}$) region and showed identical $g_{\|}$ values at 2.26–2.28 with $g_{\perp}$ values of 2.04–2.05 for all complexes (Fig. 2, Table 2). We

Table 2 Electronic spectral parameters of copper(II) complexes

Complex	Electronic spectra[a] $\lambda_{max,nm}$ (ε, M^{-1} cm^{-1})	EPR parameters[b] $g_{\parallel}$	$g_{\perp}$	$A_{\parallel}$ (cm^{-1})	$A_{\perp}$	f(cm)	α^2	β^2	γ^2	$K_{\parallel}$	$K_{\perp}$	K
1	222 (28 800) 305 (7800) 374 (11 800) 680 (32)[b] 887 (20)	2.27[c] 2.26[d]	2.04[c] 2.04	154[c] 148[d]	9.5	147	0.7519	0.8821	0.7686	0.6750	0.5781	0.6370
2	224 (31 800) 300 (15 000) 375 (31 800) 710 (34) 885 (25)	2.26[c] 2.25[d]	2.05[c] 2.05[d]	139[c] 150[d]	9.5	162	0.7041	0.9416	0.9032	0.6631	0.6360	0.5530
3	222 (45 600) 294 (17 000) 377 (20 200) 725 (32) 882 (23)	2.28[c] 2.28[d]	2.05[c] 2.04[d]	163[c] 168[d]	9.5	140	0.7908	0.8718	0.7971	0.6894	0.6303	0.6774
4	222 (51 000) 306 (32 600) 384 (16 600) 741 (46) 932 (34)	2.27	2.04	153	9.5	148	0.7489	0.8799	0.7397	0.6591	0.5540	0.6344

[a] Concentration 1×10^{-2} M in acetonitrile/HEPES buffer pH 7.34 at 25 °C. [b] Measured at 70 K in methonal : DMF(8 : 2); $A_{\parallel}$ and $A_{\perp}$ 10^{-4} cm^{-1}. $f = (g_{\parallel}/A_{\parallel})$, $\alpha^2 = A_{\parallel}/0.036 + (g_{\parallel} - 2.0023) + 3/7\ (g_{\perp} - 2.0023) + 0.04$. $K_{\parallel} = \alpha^2\beta^2$ and $K_{\perp} = \alpha^2\gamma^2$, $K_{\parallel}{}^2 = (g_{\parallel} - 2.0023)\ \Delta E\ (d_{xy} - d_{x^2-y^2})/8\lambda_0)$, $K_{\perp}{}^2 = (g_{\perp} - 2.0023)\ \Delta E(d_{xz,yz} - d_{x^2-y^2})/2\lambda_0)$, $K_{\parallel} = \alpha^2\beta^2$, $K_{\perp} = \alpha^2\gamma^2$, $\beta^2 = K_{\parallel}/\alpha^2$, $\gamma^2 = K_{\perp}/\alpha^2$, $K = A_{iso}/P\beta^2 + (g_{av} - 2.0023)/\beta^2$. [c] Experimental value. [d] Calculated value from simulated spectra.

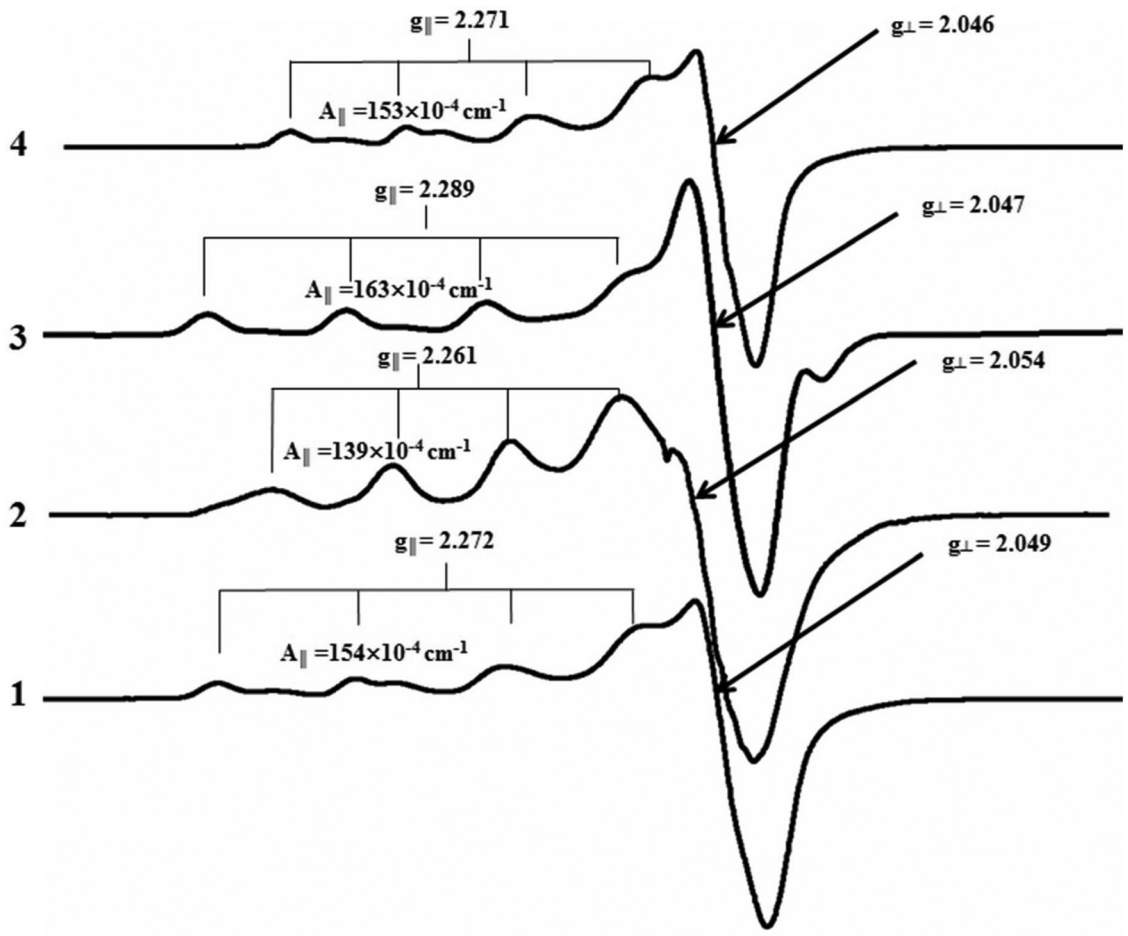

Fig. 2 EPR spectra of **1–4** in a methanol/DMF mixture at 70 K. Microwave frequency, 9.647 GHz; microwave power, 1.0 mW; modulation amplitude, 10 G; modulation frequency, 100 kHz; time constant, 40.96.

found $g_{\|} > g_{\perp} > 2.0023$, suggesting an unpaired electron on the $d_{x^2-y^2}$ orbital with the $^1B_{2g}$ ground state.[30] Even though the highest-energy singly occupied d-orbital was $d_{x^2-y^2}$ its lobes may not have been pointing directly at the ligands, which resulted in a smaller repulsive or antibonding interaction with the ligand field as compared with perfect square-based geometry.[31] All the complexes exhibited *f*-values ($g_{\|}/A_{\|}$) of 140–162 cm^{-1}, which were higher than those of square-based geometries (105–135 cm^{-1}).[32,33] The higher *f*-values revealed larger distortion in coordination geometry, suggesting strong deviation from planarity.[33] The line from minor *g*-values at 2.43, 2.31 for **1**, 2.42, 2.29, 2.16 for **3**, and 2.46, 2.32 for **4** corresponded to an additional minor species that may have originated from solvation and exchange of coordinated water molecules with anions[34] or from geometrical interconversion.[35] However, these minor species could not be discriminated by the electronic absorption spectra in acetonitrile, methanol, DMF or in a methanol–DMF mixture (Fig. S6†). Electrospray ionization-mass spectrometry (ESI-MS) of these solutions revealed mass signatures only for the core $[Cu(L)_2]^{2+}$. A spectral pattern for the 1 : 1 stoichiometry of ligand and copper(II) ions was not observed. Conversely, a minor component at 2.071 at a lower field was observed only for **2** because $M(I) = -3/2$.[36] The values of $g_{\|}$ (2.26–2.28) and $A_{\|}$ (139–163 × 10^{-4} cm^{-1}) further supported the notion of geometrical distortion with a very weak axial interaction in solution. The distortion in the square plane may have been caused by axial interaction by increasing $g_{\|}$ values and decreasing $A_{\|}$ values. The lower values of hyperfine coupling $A_{\|}$ may have been contributed from strong Fermi contact, spin dipoles and orbital dipoles.[37] Normally, the square-based CuN_4 chromophore is expected to show $g_{\|}$ and $A_{\|}$ values of 2.200 and 200 × 10^{-4} cm^{-1}, respectively.[38] The deviation of square-based geometries agreed well with solid-state structural parameters calculated from single-crystal X-ray analysis, whereby the non-zero τ-values correspond to strong distortion in coordination geometry.[38] In fact, the lower $A_{\|}$ value of **2** (139 × 10^{-4} cm^{-1}) was in good agreement with larger a geometrical distortion parameter τ (0.87) in the solid state. The lower $A_{\|}$ value of **2** was due to the larger distortion in a square plane around copper(II) centers.[39] Conversely, other complexes exhibited a relatively higher $A_{\|}$ value (153–163 × 10^{-4} cm^{-1}) and relatively smaller geometrical distortion parameter τ (0.68–0.75) than **2** in the solid state.

The EPR parameters and energy of d–d transitions were used to estimate bonding parameters such as covalency of in-plane σ-bonds (α^2), in-plane π-bonds (β^2) and out-plane π-bonds (γ^2).[40] The complex **2** exhibited lower α^2 (0.7041) and higher β^2 (0.9416) and γ^2 (0.9032) than those of **1**, **3** and **4** (Table 2). These data suggested a slightly higher degree of covalent bonding character in Cu–N bonds of **2** than that in other complexes; in general, α^2 values would be close to unity for ionic bonding and decrease with increasing covalency.[41] The orbital reduction factors $K_{\|} = \alpha^2\beta^2$ and $K_{\perp} = \alpha^2\gamma^2$ were calculated as 0.6631 and 0.636 for **2** and were almost identical to those of **1**, **3** and **4**. All the complexes showed $K_{\|} > K_{\perp}$, thereby revealing the persistence of a significant amount of out-of-plane π-bonding in all complexes, whereas $K_{\|} = K_{\perp}$ for pure σ-bonding and $K_{\|} < K_{\perp}$ in-plane π-bonding have been reported.[40] The Fermi contact hyperfine interaction term (*K*) was calculated as 0.553 for **2**, indicating an almost identical degree of covalent bonding character in Cu–N as predicted from α^2 values.[41] The *K* value is also a measure of the s-electron contribution to the hyperfine interaction.[42] The *K* value of **2** was lower than those of **1**, **3** and **4**.

The d–d transition appeared at 680 nm (ε, 32 M^{-1} cm^{-1}) for **1** in acetonitrile : HEPES [4-(2-hydroxyethyl)-1-piperazineethanesulfonic acid] buffer at pH, 7.34 (1 × 10^{-2} M) and its ligand-based transitions were merged (Table 2). The position of the d–d transition was slightly varied for **2** (710 nm, ε, 34 M^{-1} cm^{-1}), **3** (725 nm, ε, 32 M^{-1} cm^{-1}) and **4** (741 nm, ε, 46 M^{-1} cm^{-1}). The energy order of d–d transitions was **1** > **2** > **3** > **4**. The energies of d–d transitions supported the existence of five-coordinate geometry with $d_{x^2-y^2}$ ground state in all complexes.[40,43] Also, low-energy shoulders observed around 882–932 nm for **1–4** could be attributed to d–d transitions characteristic of distorted square-pyramidal geometry,[44] which is due to geometrical interconversion in solution. Interestingly, the solid-state absorption spectra of **1–4** showed d–d transitions around 735–787 nm and their positions were slightly shifted from the respective solution spectra (Fig. S7†). The energies of d–d transitions were not significantly affected while complexes interacted with selected amino acids such as alanine, arginine, glycine, histidine, leucine, proline, serine, threonine, tryptophan, and tyrosine in acetonitrile : HEPES buffer at pH, 7.34. Interestingly, while interacting, the complexes with Cys caused an immediate disappearance or huge decrease in intensity of d–d transitions due to the instantaneous reduction of Cu(II) into Cu(I) (Fig. S8†). In particular, the d–d transition of **2** was decreased gradually by the measured addition of Cys and completely quenched by 5 equivalents (Fig. 3). The solution turned yellow and after while

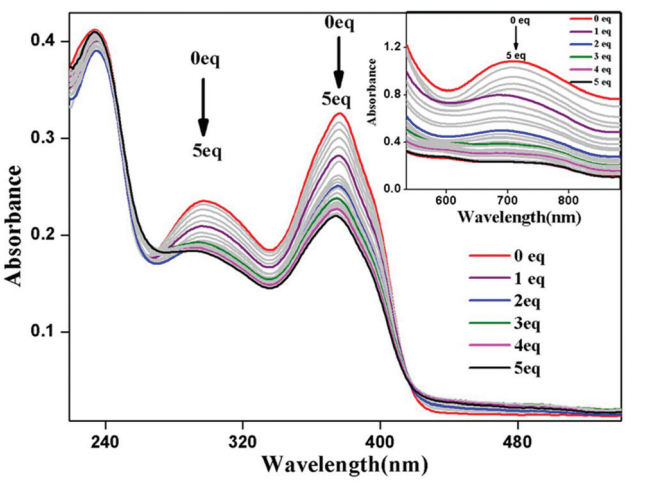

Fig. 3 Electronic spectral changes upon addition Cys to **2** (5 × 10^{-6} M) in HEPES buffer (pH 7.34) at 25 °C. Inset: Depletion of a d–d band of **2** by addition of Cys (10^{-2} M) in DMF HEPES buffer.

caused a colorless precipitate corresponding to Cys-bound Cu(I) complexes (Fig. S9†), which was characterized by HR-MS, ^{1}H NMR, infrared (IR) and elemental analysis. HR-MS spectra showed a molecular ion peak at *m*/*z*, 785.3256 corresponding to $[Cu^{I}(L)_2(Cys)]$ (Fig. S10†). The element composition was measured by elemental analysis, and found to be, for $CuC_{41}H_{36}N_7O_4S$, the following: C, 62.60; H, 4.60; N, 12.44. This was similar to the calculated elemental composition (C, 62.62; H, 4.61; N, 12.47). This notion was further supported by ^{1}H NMR, whereby the formation of Cu(I) was accompanied with a shift in the α-CH and β-CH_2 resonances of Cys towards a higher field along with ligand spectral signatures. α-CH and β-CH_2 protons appeared at 3.99 and 3 ppm for free Cys, respectively.[45] One equivalent of Cys with **2** showed a broadening of ^{1}H NMR peaks, possibly due to a mixture Cu(II) and Cu(I) species. However, addition of 5 equivalents exhibited well-resolved ^{1}H NMR peaks corresponding to $[Cu^{I}(L)_2(Cys)]$ (Fig. S11†). The observed chemical-shift values of Cys were similar to those of previously reported Cu(I)-Cys complexes.[45] The IR stretching frequencies ($\bar{\nu}$) appeared at 2915, 1577, 1482 and 1401 cm^{-1}, which showed considerable shifting from free Cys, and matched with $\bar{\nu}_{st}$ of Cu^{I}-(Cys) (Fig. S12†).[46] Interestingly, treatment of $[Cu^{I}(L)_2(Cys)]$ with one equivalent of H_2O_2 (30%) resulted in regeneration of the original d–d band of **2** at 693 nm (ε, 26 M^{-1} cm^{-1}) and further addition of Cys led to disappearance of the d–d band again. This result clearly suggested that the interaction of Cys proceeded through the reduction of Cu(II) to Cu(I) without ligand displacement (Fig. S13†). Conversely, our previously reported rigid Cu(II)-complexes could not yield Cys-bound Cu(I) complexes, whereas ligand displacement was noticed after reduction of the Cu(II) center.[11,27]

The ligand-based π–π* transitions of **1** were resolved at lower concentration (5×10^{-6} M) and showed three major absorption bands around 222 nm (ε, 28 800 M^{-1} cm^{-1}), 305 nm (ε, 7800 M^{-1} cm^{-1}) and 374 nm (ε, 11 800 M^{-1} cm^{-1}) in HEPES buffer at pH 7.34. The energy of these transitions was not significantly affected by ligand architecture and almost identical spectral signatures were observed for **2–4** (Fig. S14†). However, their intensities were notably increased by introducing electron-releasing methoxy and dimethylamine groups on the phenyl rings of **1** to obtain **2** and **4**, respectively, and caused redshift. The interaction of selected amino acids with **1**, **3** and **4** showed almost no change or slight shift or change in the intensity of transitions at this lower concentration. This may have been due to weaker coordination or coordination without major geometrical rearrangements and the oxidation state (*cf.* below) of the copper(II) center. Interestingly, the interaction of Cys with **2** showed significant spectral changes. Nevertheless, the other amino acids mentioned above almost unaltered the absorption spectral signatures of **2**. The stability and formation of **2** were examined by monitoring absorption spectral changes at this biologically relevant lower concentration (5×10^{-6} M). The gradual addition of Cu^{2+} to L2 resulted in the disappearance of the ligand-based transitions at 317 (ε, 28 500 M^{-1} cm^{-1}) and 360 nm (ε, 22 860 M^{-1} cm^{-1}) in HEPES buffer at pH, 7.34. This was accompanied by the simultaneous appearance of new bands around 224 nm (ε, 31 800 M^{-1} cm^{-1}), 300 (ε, 15 000 M^{-1} cm^{-1}) and 375 nm (ε, 31 800 M^{-1} cm^{-1}) corresponding to formation of **2** (Fig. S15†). The formation of **2** was further confirmed by HR-MS, whereby a molecular ion peak appeared at *m*/*z* = 814.12347, corresponding to $[Cu(L2)_2(SO_3CF_3)]^+$. The stability constant was calculated as 9.04 by pH-metric titration (Fig. S16†). The interaction of **2** (5×10^{-6} M) with Cys as a function of concentration was studied by following changes in ligand field transitions. The bands at 300 (ε, 15 000 M^{-1} cm^{-1}) and 375 nm (ε, 31 800 M^{-1} cm^{-1}) were decreased gradually over the calculated addition of Cys, and saturated at 5 equivalents. This observation clearly showed that only Cys could alter the absorption pattern of **2** *via* reduction of Cu(II) into Cu(I), and led to the formation of $[Cu^{I}(L)_2(Cys)]$ (*cf.* above). After this formation, coordinated Cys possibly oxidized to attain formation of the Cys-S-S-Cys bond, and then dissolved oxygen likely to facilitate the re-oxidation of Cu(I) for the binding of next Cys.[47] The addition of other biomolecules, such as homocysteine, glutathione, and methionine, showed relatively negligible changes in the absorption spectrum of **2**. Also, the absorption spectral pattern of **2** was unaltered by the addition of 10 equivalents of biologically relevant cations (K^+, Ca^{2+}, Mg^{2+}, Mn^{2+}, Fe^{2+}, Fe^{3+}, Co^{2+}, Ni^{2+}, and Zn^{2+}) and anions such as sulfate and phosphate, at pH = 7.34 (Fig. S17†). Thus, probe **2** was stable enough for imaging under biological conditions without transmetalation or interferences by endogenous metal ions or anions at this pH.

Redox studies

The redox behavior of complexes was investigated by cyclic voltammetry (CV) using a three-electrode cell configuration and NaCl as the supporting electrolyte in HEPES buffer solution at pH 7.34. A platinum sphere, platinum wire, and Ag/Ag^+ were used as the working, auxiliary, and reference electrode, respectively. The measured redox potentials were converted into a normal hydrogen electrode (NHE) by adding +0.205 V.[27] The Cu(II)/Cu(I) redox potential of probe **1** (0.221 V *vs.* NHE) was lower than that for **4** (0.525 V *vs.* NHE) but almost identical to that of **2** (0.237 V) and **3** (0.218 V) (Table 3, Fig. S18†). The Cu(II)/Cu(I) redox potentials of **1–4** were higher than the biological redox potential ranges. In healthy differentiated cells, the glutathione/glutathione disulfide (GSH/GSSG) redox couple was approximately −0.22 V *vs.* NHE, but became more reducing in proliferating cells (−0.26 V), which corresponded to a higher GSH : GSSG ratio. The extracellular redox potential of the cysteine/cysteine disulfide (CySH/CySSCy) couple is typically −0.080 V, whereas pathologic cells demonstrate CySH/CySSCy potentials ranging from −0.062 to −0.02 V in the extracellular space.[48] The treatment of Cys with **1**, **3** and **4** displayed only slight changes in Cu(II)/Cu(I) redox potentials. Nevertheless, the Cu(II)/Cu(I) redox potential of **2** shifted to a more negative potential by the reaction of Cys ($E_{1/2}$, 0.190 V *vs.* NHE; ΔE, 89 mV). It was studied further by electrochemical titration, whereby the gradual addition of Cys to **2** (1×10^{-3} M)

Table 3 Optical and redox data for **1–4**

	Redox data[a]					Emission data		
Complex	E_{pa} (V)	E_{pc} (V)	ΔE (mV)	$E_{1/2}$ (V)	$E_{1/2}$ (V, *vs.* NHE)	λ_{emi}[e] (nm)	Binding constant[f]	Detection limit[f]
1	0.062	−0.030	92	0.016	0.221	490	1×10^5	1.9×10^{-7}
	0.339	0.26	79	0.299[b]	0.504			
2	0.070	−0.007	77	0.032	0.237	467	2.3×10^5	9.9×10^{-8}
	0.003	−0.059	89	−0.015[b]	0.190			
	0.019	−0.057	76	−0.019[c]	0.186			
	0.08	−0.024	104	0.028[d]	0.217			
3	0.057	−0.032	89	0.0125	0.218	460	1.3×10^4	1×10^{-7}
	0.040	−0.032	72	0.004[b]	0.209			
4	0.356	0.284	72	0.320	0.525	465	1.6×10^4	1.5×10^{-7}
	0.365	0.250	115	0.307[c]	0.512			

[a] Concentration 1×10^{-3} M in HEPES buffer pH 7.34 at 25 °C (reference: saturated Ag/Ag^+; supporting electrolyte: 0.1 M NaCl solution; scan rate = 50 mV s^{-1}). To convert $E_{1/2}$ *vs.* NHE add +0.205. [b] Complex + Cys. [c] Complex + His. [d] Complex + GSH. [e] Corresponding to respective ligands. [f] Calculated in HEPES buffer pH 7.34 at 25 °C.

showed a shift in the Cu(II)/Cu(I) redox potential, along with increases of current values up to one equivalent (Fig. S19a and b†). Further addition of Cys resulted in a gradual shift in redox potential with a decrease in current values. These changes were linear up to seven equivalents of Cys and then started precipitating a colorless solid (Fig. 4). The solid was characterized as $[Cu^I(L2)_2(Cys)]$ by HRMS and IR spectroscopies (*cf.* above). The formation of Cys-bound reduced species $[Cu^I(L2)_2(Cys)]$ was interesting and different from our previous observation, whereas the Cu(I) ion was displaced from the coordination sphere and released free ligands.[11,27] A completely different redox behavior was noted for the reaction of $Cu(SO_3CF_3)_2$ with Cys under an identical condition, whereby the Cu(II)/Cu(I) redox couple disappeared readily (Fig. S20†). Conversely, electrochemical titration of **2** with histidine (His) exhibited only a slight shift in Cu(II)/Cu(I) redox potential with significant decreases in current values without concomitant reduction, which may have been due to the coordination of His (Fig. S21a†). This result was supported further by the persistence of the d–d band after the interaction of **2** with His (Fig. S22†). The binding constant (K) for the interaction of **2** and His was calculated to be 6.7×10^4 M^{-1} (Fig. S23†). Also, an non-significant change in Cu(II)/Cu(I) redox potentials was observed for the addition of five equivalents of GSH to **2**, but the current value decreased (Fig. S21b†). The other amino acids could not produce such electrochemical changes under identical conditions.

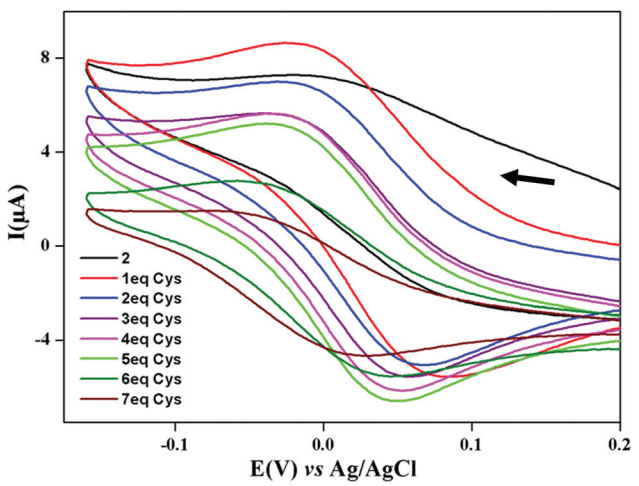

Fig. 4 Electrochemical titration of $[Cu(L2)_2(CF_3SO_3)_2]$ **2** (1×10^{-3} M) with various amounts of Cys using NaCl as the supporting electrolyte in HEPES buffer at pH 7.34.

Optical spectral studies

The ligands L1–L4 showed strong fluorescence in the range 460–490 nm in HEPES buffer at pH 7.34 (5×10^{-6} M) and the energy of their emission wavelengths were strongly influenced by electronic substituents. The fluorescent quantum yields of the ligands were calculated to be 4%, 3.8%, 7.6% and 1.1% for L1, L2, L3 and L4, respectively (Table S1†). However, their copper(II) complexes were found to be non-fluorescent. This 'turn off' behavior emerged due to the paramagnetic Cu(II) center.[11,27] Specifically, the fluorescence intensity of the ligand L2 was completely quenched by the coordination of Cu^{2+}. The binding constant for Cu^{2+} and L2 was calculated as 5.3×10^6 (Fig. S24†). This finding was supported further by the highest occupied molecular orbital/lowest unoccupied molecular orbital (HOMO–LUMO) electron density map of **2**. Computational calculations were carried out using B3LYP, 6-31G (for C, H, N, and O) and TD-DFT using LANL2DZ (for Cu) basis sets in the Gaussian 09 program[49] (Fig. S25, Table S2†). The frontier molecular orbital analysis of L2 revealed the HOMO to be localized on the entire ligand moiety, and LUMO to be localized only on the imidazopyridine moiety. However, for **2**, the HOMO localized around the imidazopyridine moiety and LUMO was localized around the pyridine moiety and copper center. This scenario was due to the collapse of the electronic conjugation of the ligand by the Cu^{2+} center through internal charge transfer. That is, the electron density localized on the ligand moiety was transferred to the copper(II) center. After the interaction of Cys with **2**, the HOMO localized

around copper and Cys, and the LUMO localized around the imidazopyridine moiety. A larger HOMO–LUMO energy gap for **2** (3.125 (2) eV) referred to higher kinetic stability and lower chemical reactivity.[50] Single-excitation time-dependent DFT (TDDFT) was undertaken to explain the electronic structural properties of the ground and excited states of **2**. The vertical transitions calculated by TDDFT were comparable with the experimentally observed electronic spectra of **2**, whereby the vertical $\pi \rightarrow \pi^*$ transition at ~370 nm was almost closer to the experimentally observed spectra at ~375 nm.[51] They corresponded to the pure HOMO → LUMO+1 excitation. The LUMO+1 localized around imidazopyridine and the copper center. However, after the interaction of Cys with **2**, the LUMO localized around the imidazopyridine moiety and the HOMO was transferred to copper and cysteine. The experimentally absorbed $\pi \rightarrow \pi^*$ transition spectra at 375 nm for **2** + Cys corresponded to the HOMO−1 → LUMO excitation.

The emission property of **1**, **3** and **4** was altered by the interaction of selected amino acids (Fig. S26†) and turned on their fluorescent intensity without selectivity. In particular, the interaction of Cys and His with **1**, **3** and **4** showed huge fluorescent enhancement compared with that for other listed amino acids. Amazingly, the probe **2** exhibited turned-on fluorescent behavior only by the interaction of Cys, however, it remained non-fluorescent with all other amino acids. The intensity raised by **2** with Cys was 103-fold higher than its original intensity (Fig. 5a). The fluorescence intensity increased linearly upon gradual addition of Cys (Fig. S27†) and this intensity enhancement was saturated at 12 equivalents. Then, the intensity remained unchanged up to 17 equivalents (Fig. S28†). The binding constant (K) for the interaction of **2** and Cys was calculated as 2.3×10^5 M^{-1} from the linear plot obtained using the Benesi–Hildebrand expression, $I_o/I - I_o = b/(a - b)\{1/K[M] + 1\}$; where I_o and I are the intensities in the absence and presence of the analyte, respectively, [M] is the concentration of the analyte, and 'a' and 'b' are the intercept and slope of the plot, respectively. The linear plot was obtained by fitting $(I_o/I - I_o)$ *versus* 1/[M].[52] The limit of detection was calculated as 9.9×10^{-8} M by employing the formula [3× (standard deviation/slope)] to the linear plot. However, other complexes exhibited a lower binding constant with Cys (1.3×10^4 to 1×10^5) as compared with **2** (Table 3). A Job's plot was obtained by fluorescence titration of **2** with Cys and revealed one equivalent binding of Cys (Fig. S29†). The biological redox buffer glutathione (GSH) and homocysteine (Hcys) could not produce similar fluorescent enhancement even though they contain a thiol group. Their enhancement of fluorescent intensity was very much lower even with 10 equivalents, which was negligible as compared with the intensity raised by Cys under identical conditions (Fig. 5b). This disparity was due to the higher pK_a values of GSH (9.2), Hcys (10.0), than L-cysteine (8.3),[53] and they are expected to show weaker coordination with **2** than Cys and, hence, the reduction of Cu(II) to Cu(I).[54] In fact, the fluorescence intensity of **2** was not raised even with 10 equivalents of the other listed amino acids. However, the addition of one equivalent Cys to the same solution raised the

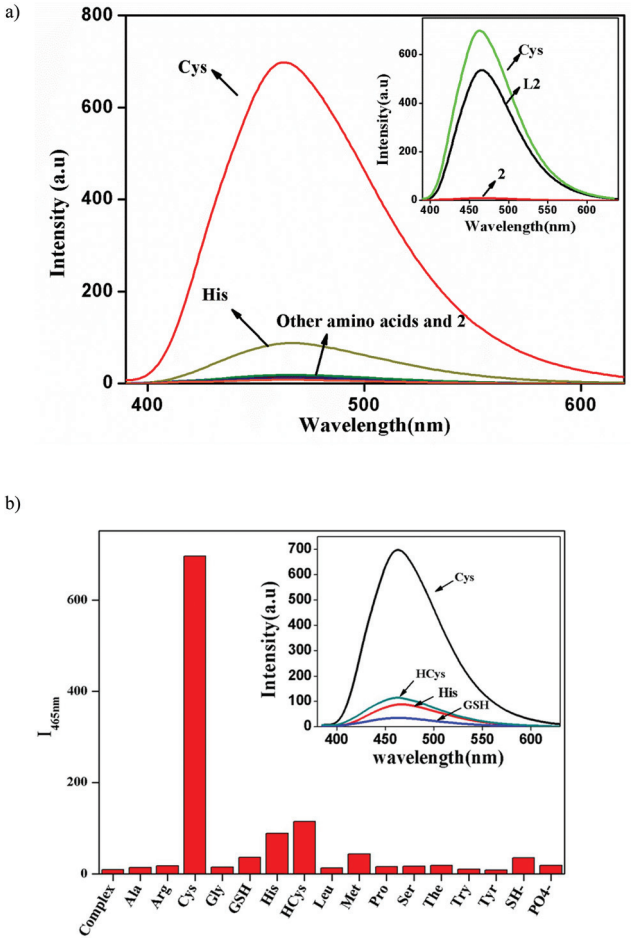

Fig. 5 (a) Fluorescence spectra of **2** (5×10^{-6} M) with various amino acids (5×10^{-5} M) in HEPES buffer pH, 7.34 at 25 °C. Inset: Fluorescence spectra of L2, **2**, **2** + Cys. (b) Bar diagram for the selectivity of various amino acids and biologically relevant ions. Inset: Fluorescence spectra of **2**, **2** with HCy, His, GSH (5×10^{-5} M, λ_{ex} = 367 nm).

fluorescence intensity immediately (Fig. 6). This finding suggested that **2** was highly sensitive toward Cys and able to be visualized even at lower concentrations. There was no concomitant change in the fluorescence intensity of **2** over the pH range 4.5–9.5. However, **2** with Cys showed gradual increment in intensity on increasing pH up to 9.5 (Fig. S30†). The fluorescence intensity of **2** was not enhanced by biological cations (K^+, Ca^{2+}, Mg^{2+}, Mn^{2+}, Fe^{2+}, Fe^{3+}, Co^{2+}, Ni^{2+}, and Zn^{2+}) at pH 7.34 (Fig. S31†). This clearly ruled out the possibility of transmetalation in **2** by these biologically relevant cations.[55] Also, the fluorescence intensity of **2** was not turned on by adding biological anions such as SH^-, PO_4^{3-}, SO_4^{2-} or H_2S (Fig. S32†). Similar to absorption spectral studies, addition of one equivalent H_2O_2 (30%) to the solution of $[Cu^I(L2)_2(Cys)]$ led to immediate quenching of fluorescence intensity due to the oxidation of Cu(I) to Cu(II) (Fig. S33†) (Scheme 2) and it was regenerated by addition of another equivalent of Cys. The enhancement of fluorescence intensity by Cys may have occurred *via* two consecutive steps. First, the copper(II) center was reduced

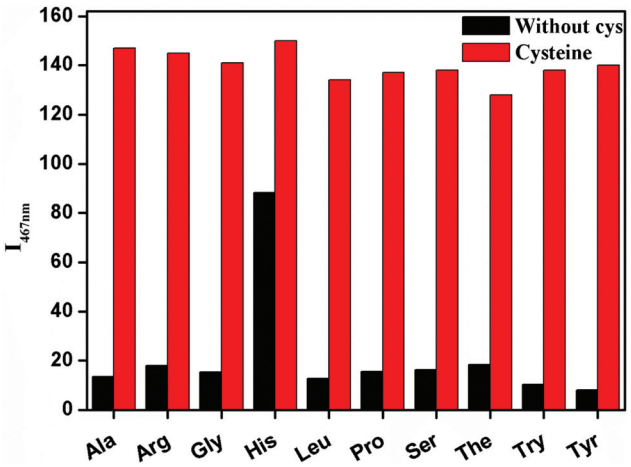

Fig. 6 Competitive binding experiments of **2** (5×10^{-6} M) with various amino acids (5×10^{-5} M) in the absence (black) and presence of one equivalent Cys (red) in HEPES buffer pH, 7.34 at 25 °C.

to copper(I) by Cys, as expected. Once reduced, the copper(I) ion apparently requires trigonal-based coordination geometry.[56] The reduction presumably involves significant geometrical reorganization through internal changes in the bond lengths and angles. In the Cys ligand, the sulfur atom has three valence 3p orbitals: one of the p-orbitals is used for a C–S bond and the remaining two degenerate p-orbitals are perpendicular to the C–S bond. The two degenerate p-orbitals can interact with the copper center and split in energy depending on the C–S–Cu angle. By changing the C–S–Cu angle *via* the interaction between the S-pπ-orbital and Cu-$d_{x^2-y^2}$ orbital, a tetrahedral/tetragonal similar to the Cu–S interaction of blue Cu-proteins can be adopted.[57] While the interaction is weakening, the maximum absorption peak is shifted to higher energy and *vice versa*. The required geometrical plasticity for the coordination of Cu(II) and Cu(I) ions may be better stabilized by the *p*-substituted methoxy group of **2**. A nearly-perfect trigonal plane of **2** (predicted by a lower $A_{||}$ in EPR and molecular structure) enforced faster electron transfer and selectivity as compared with other complexes. In fact, it showed a higher binding constant with Cys among the other complexes. The distorted trigonal plane adopted in **1**, **3** and **4** may require higher reorganization energy for electron transfer and, hence, reduction of Cu(II) to Cu(I) by Cys[58] and possibly led to poor selectivity.

Imaging of living cells

The optical imaging probe **2** could visualize Cys selectively in an isolated chemical environment as established by spectral and redox methods. Thus, it provided suitable excitation/emission wavelengths and brightness for Cys imaging in living cells. First, MTT [3-(4,5-dimethylthiozol-2-yl)-2,5-diphenyltetrazolium bromide] assays were carried out for Henrietta Lacks cervical cancer (HeLa) cells and macrophage cells, and calculated as 86.26% and 75.26%, respectively. They exhibited low cytotoxicity limits with cell viability up to 75 μM concentration (Fig. 7). This finding suggested that probe **2** could be explored as a biomarker for imaging Cys in living cells without affecting their viability. Therefore, we investigated the Cys imaging ability of probe **2** in HeLa cells and macrophages *via* a turn-on fluorescent mechanism under physiological pH (7.34). HeLa

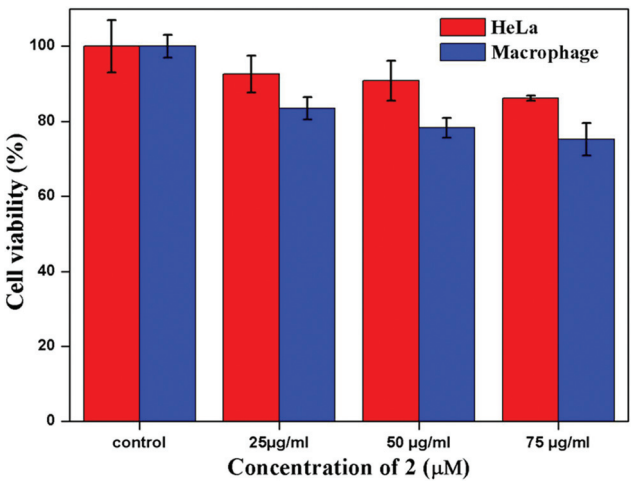

Fig. 7 MTT assay in HeLa cells. Mean ± standard error from the tested triplicate samples is represented as mean error bars. HeLa cells (red) and macrophages (blue) were incubated with 0–75 μM of **2** for 24 h.

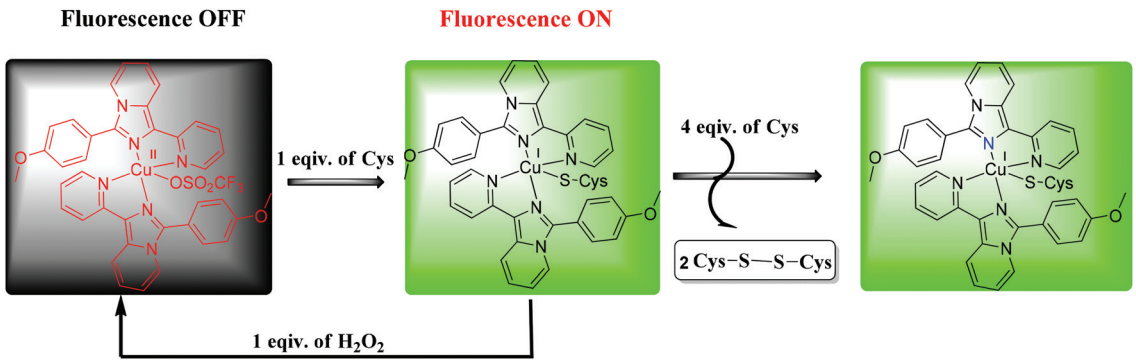

Scheme 2 The reaction of **2** with Cys in HEPES buffer at pH 7.34.

and macrophage cells were incubated with **2** (5 μM) for 30 min at 37 °C. Monolayers of two cells were grown on cover-glass Petri dishes for the measurement of fluorescence and bright-field images. Then, laser scanning fluorescence microscopy was done at an excitation wavelength of 367 nm using green filter. Acridine orange was used as a fluorescent intercalating agent. HeLa cells showed reasonable brighter fluorescence images, possibly corresponding to the amount of Cys in living cells. HeLa cells were pre-treated with 100 μM of Cys over 30 min at 37 °C followed by incubation with **2** (5 μM) for an additional 30 min. The imaging of HeLa cells by laser scanning fluorescence microscopy exhibited brighter fluorescence images as compared with images from untreated cells. These results clearly suggested that probe **2** could interact directly with Cys in a transient manner through cell membranes at biological pH (7.34) and reduce the copper(II) center into copper (I). However, pre-treatment of a thiol-blocking agent (200 μM of *N*-ethylmaleimide (NEM)) with HeLa cells before addition of **2** (5 μM) showed only a very faint fluorescence image. Before treatment with **2**, the cells showed almost no fluorescence in a similar region. The Cys imaging experiment was also examined for macrophage cell lines to enable comparison of the efficiency and specificity of probe **2**. Macrophage cell lines also showed almost similar fluorescence images (Fig. 8 and S34†) before and after exogenous treatment with Cys. These imaging studies on living cells revealed that **2** could enter cancer cells and turn on fluorescence intensity by detecting Cys. Interestingly, probe **2** showed no significant changes in cell structure or morphology under our experimental conditions.

Summary

The copper(II) complexes of imidazopyridine-based ligands were synthesized as an optical imaging probe for visualizing Cys in cancer cells. The molecular structure of the complexes adopted a distorted trigonal pyramidal around copper(II) centers in the solid state. This five-coordinate geometry also persisted in solution, as supported by electronic spectral data. Interestingly, the complex with a *p*-methoxy substituent on phenyl rings adopted a nearly perfect trigonal plane around the copper(II) center, which facilitated faster reduction of Cu(II) to Cu(I) selectively by Cys. Other complexes exhibited strong distortion around the trigonal plane (which may require higher reorganization energy for electron transfer and reduction of Cu(II) to Cu(I)) and resulted in poor selectivity.

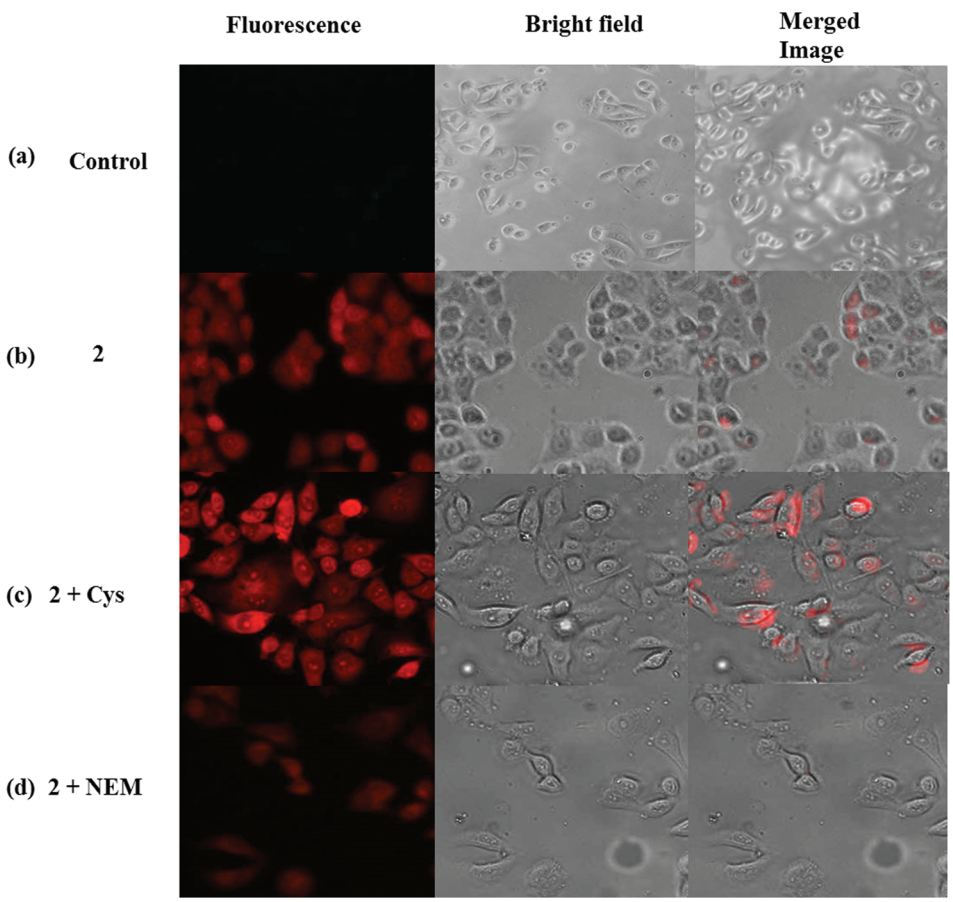

Fig. 8 Fluorescence and bright-field images of HeLa cells: (a) cells in the absence of **2**, (b) cells incubated with **2** (5 μM) for 30 min, (c) cells pre-treated with 100 μM Cys and incubated with **2** (5 μM) for 30 min, and (d) cells pre-treated with 200 μM NEM and incubated with **2** (5 μM) for 30 min.

The Cu(II)/Cu(I) redox potential of the complexes varied slightly by ligand electronics, whereby methoxy substituents on phenyl rings showed a lower redox potential than that of $-NMe_2$ substituents. All ligands exhibited strong fluorescence, but their copper(II) complexes were non-fluorescent. The emission behavior of complexes varied significantly upon interactions of amino acids, and turned on their fluorescent intensity without selectivity. Interestingly, one of the probes with *p*-methoxy substituents showed a selective turn-on fluorescence property towards Cys over other amino acids. It showed an excellent binding constant of 2.3×10^5 M^{-1} and a limit of detection of 9.9×10^{-8} M at pH 7.34. The probing mechanism of Cys likely operated *via* reduction of copper(II) to copper(I) without ligand displacement. After reduction, the electronic conjugation was regenerated and fluorescence intensity enhanced at the bright visible region. Furthermore, this probe exhibited significantly brighter fluorescence images for living cells such as HeLa and macrophage cell lines. The intensity of the images was enhanced by exogenous addition of Cys to living cells. Cell-imaging experiments strongly suggested that our probe might cross membrane barriers readily to permeate into living cells rapidly for imaging intracellular Cys with low cytotoxicity.

Experimental section

Materials

Unless indicated otherwise, common reagents or materials were obtained from a commercial source and used without further purification. All solvents were used after appropriate distillation or purification. The chemicals 3,4-dimethoxybenzaldehyde, di-pyridin-2-yl-methanone, copper(II) chloride, copper(II) triflate, zinc(II) chloride, cobalt(II) chloride, iron(II) chloride, iron(III) chloride, magnesium(II) chloride, manganese (II) chloride, calcium chloride, sodium chloride, potassium chloride, L-alanine, L-arginine, L-cysteine, L-glycine, L-histidine, L-leucine, L-proline, L-serine, L-threonine, L-tryptophan, L-tyrosine, L-methionine, DL-homocysteine, L-glutathione, sodium phosphate and methyl mercaptoacetate were purchased from Sigma-Aldrich. NH_4OAc was obtained from Merck.

Physical measurements

All reactions were carried out under an atmosphere of dry nitrogen. Glassware was oven-dried prior to use. Unless indicated otherwise, common reagents or materials were obtained from a commercial source and used without further purification. All solvents were used after appropriate distillation or purification. EPR spectra were recorded at 77 K using a JEOL X-band spectrometer (JES-FA100). The spectra simulation was carried out using JEOL Anisotropic Simulation software (AniSim/FA). NMR spectra were recorded at 400 MHz using a Bruker spectrometer. Chemicals-shift values and coupling constants are given in ppm and Hz, respectively. HR-MS spectra were measured on a Thermo Scientific Exactive Plus EMR instrument. Elemental analyses were carried out using a Heraeus Vario Elemental automatic analyzer. Fourier transform-infrared (FT-IR) measurements were carried out using a Nicolet 6700 system. Absorption spectra were undertaken using Agilent Technologies diode array 8453 spectrometers at 298 K, and emission spectra were measured on an Agilent Technologies Cary Eclipse spectrofluorometer at 298 K. Electrochemical data were recorded in a Biologic SP-150 Electrochemical Workstation using saturated Ag/Ag^+ and Pt as a reference electrode and working electrodes, respectively; 0.1 M NaCl was used as a supporting electrolyte. The electrodes are calibrated by $K_4[Fe(CN)_6]$ prior to measurements.

Determination of X-ray structure

These experiments were carried out on an Agilent Technologies Supernova-E CCD diffractometer. Single crystals of suitable size were selected from the 'mother' liquor and immersed in paraffin oil, then mounted on the tip of a glass fiber. A Mo radiation source and microfocus tube multilayer mirror optics (λ = 0.71073 Å) were used for data collection. The structures were solved by direct methods using the program SHELXS-2013. Refinement and all further calculations were carried out using SHELXS 2013. H-atoms were included in calculated positions and treated as 'riding' atoms using SHELX default parameters. Non-H atoms were refined anisotropically using weighted full-matrix least-square on F^2. CCDC 1833674, 1833675, 1833676 and CCDC 1833677† contained the supplementary crystallographic data for our study. Structural refinement parameters **1–4** are summarized in Table 4.

DFT methods

Geometry optimizations were undertaken using DFT methods. For metal ions, LANL2DZ basis sets with the Becke3–Lee–Yang–Parr hybrid functional (B3LYP) were used. For elements other than metals, the 6-311G (d) basis sets were employed. All DFT and TD-DFT calculations were carried out using the Gaussian 09 program package.[59]

Measurement of the stability constant

The pH of solutions was measured with an ELICO instrument (Model LI120) equipped with a combined glass electrode assembly. This instrument has a built-in internal electronic voltage supply with a temperature compensator covering the range from 0 °C to 100 °C. The instrument was calibrated with buffer solutions of acidic and basic pH before start the pH titrations. Specific solutions were used to calculate the metal–ligand stability constant over a pH range of 0–14 by 0.1 M of NaOH. The total volume (10 mL) of solution contained 0.2 mL of 0.1 M HNO_3, 2.8 mL of distilled water, 6 mL of dioxane and 1 mL of 1 M $NaNO_3$. For ligand and metal–ligand titrations, 0.5 mL of 0.1 M ligand solution and 0.1 mL of 0.1 M metal solution were used subsequently.

MTT assay using 2 for HeLa and macrophage cell lines

The MTT assay is a simple colorimetric assay to measure cytotoxicity. Metabolically active cells can convert this tetrazolium salt into a water-insoluble dark-blue formazan. The resultant

Table 4 Crystal data and structure refinement for **1–4**

	1	2	3	4
Empirical formula	$C_{40}H_{31}CuF_6N_7O_7S_2$	$C_{41}H_{34}CuF_6N_6O_{10}S_2$	$C_{42}H_{36}CuF_6N_6O_{11}S_2$	$C_{43}H_{42}CuF_6N_8O_8S_2$
Formula weight	963.38	1012.40	1042.43	1040.50
Crystal system	Triclinic	Triclinic	Triclinic	Monoclinic
Space group	$P\bar{1}$	$P\bar{1}$	$P\bar{1}$	$C2/c$
a [Å]	11.0766(9)	11.4660(8)	10.1295(7)	27.6006(14)
b [Å]	14.1661(10)	11.5674(8)	15.0236(9)	15.8879(8)
c [Å]	14.7052(10)	17.1754(11)	16.3207(10)	21.9963(12)
α [°]	69.381(6)	88.282(5)	101.942(5)	90
β [°]	75.972(6)	71.269(6)	104.135(6)	108.440(6)
γ [°]	72.748(7)	81.010(6)	98.175(6)	90
V [Å^3]	2037.7(3)	2130.4(3)	2307.3(3)	9150.5(9)
T [K]	293(2)	293(2)	293(2)	293(2)
Density [Mg m^{-3}]	1.570	1.578	1.500	1.511
Z	2	2	2	8
μ [mm^{-1}]	0.726	0.703	0.653	0.655
F (000)	982	1034	1066	4280
No. of reflections collected	12 975	14 752	10 939	29 689
Goodness of fit on F^2	1.023	1.047	1.029	1.041
R_1 [a]	0.0825	0.0951	0.1093	0.0992
wR_2 [b]	0.1460	0.2115	0.1938	0.1995

[a] $R_1 = \sum||F_o| - |F_c||/\sum|F_o|$. [b] $wR_2 = [\sum w(F_o^2 - F_c^2)^2/\sum w(F_o^2)^2]^{1/2}$.

value is related to the number of living cells. To determine cytotoxicity/viability, HeLa and macrophage cells were plated at 1×10^4 cells per well in a 96-well plate at 37 °C in an atmosphere of 5% CO_2. Cells were maintained in Dulbecco's modified Eagle's medium (DMEM) supplemented with 10% fetal bovine serum (FBS) and 100 units of penicillin–streptomycin. After cell attachment, a fresh medium containing probe **2** of varying concentrations was added. After 24 h, probe **2** was removed and the medium was added, along with MTT dye solution (0.5 mg ml^{-1}), to cells. After 4 h of incubation at 37 °C in 5% CO_2, the medium was removed and formazan crystals were solubilized in 100 μL of dimethyl sulfoxide. Absorbance was read on a microplate reader at 575 nm. The relative cell viability (%) compared with control cells was calculated by [A]test/[A]control × 100. Remarkably, the MTT assay of probe **2** towards HeLa and macrophage cell lines showed viable cells accurately at 86.26% and 75.26%, respectively, up to 75 μM of probe **2**.

Laser scanning fluorescence microscopy

The human-derived cervical cancer HeLa cell line was grown and maintained in DMEM containing 10% FBS, glutamine (0.29 g L^{-1}), sodium bicarbonate (2.2 g L^{-1}), penicillin (100 000 U L^{-1}), and streptomycin (10 mg L^{-1}) in an atmosphere of 5% CO_2–95% air at 37 °C. A monolayer of HeLa cells was grown on cover glass Petri dishes for fluorescence and bright-field images. Briefly, HeLa cells grown in DMEM were washed with phosphate-buffered saline and treated with cysteine (100 μM). Then, complex (5 μM) was added and incubation allowed to proceed for 30 min. Subsequently, NEM (200 μM) and complex (5 μM) were incubated for 30 min. Cells were fixed using 4% paraformaldehyde, incubated at 37 °C for 20 min and mounted with DPX for imaging using a Carl Zeiss laser scanning microscope (LSM 710). Fluorophores were excited using 367 nm line from an argon ion laser, and emitted fluorescence was monitored at 440 ± 2 nm.

General procedure for ligand synthesis

To a flask containing a mixture of substituted benzaldehyde (1.25 g, 7.5 mmol), di-pyridin-2-yl-methanone (0.92 g, 5.0 mmol), and NH_4OAc (1.93 g, 25 mmol) were added to 25 mL of dry acetic acid. The solution mixture was slowly heated to reflux, stirred for 16 h, cooled, and 2 mL of water was added. The solution was pumped dry, and the residue was extracted with dichloromethane/water. The organic layer was dried over anhydrous sodium sulfate, filtered, and dried. The residue was chromatographed through silica gel (ethylacetate : hexane = 1 : 3) to give a yellow powder.

3-Phenyl-1-pyridin-2-yl-imidazo[1,5-*a*]pyridine (L1). Ligand L1 was prepared by the reaction of benzaldehyde, di-pyridin-2-yl-methanone (0.92 g, 5.0 mmol), and NH_4OAc (1.93 g, 25 mmol) with addition to 25 mL of dry acetic acid (1.25 g, 7.5 mmol). Yellow solid; yield: 56%. Melting range, 92–96 °C; NMR (400 MHz, $CDCl_3$), δ 8.65–8.62 (d, 1H, py-CH, J = 12 Hz), 8.57–8.56 (d, 1H, imz-CH, J = 4 Hz), 8.20–8.17 (d, 2H, py-CH, J = 6 Hz), 7.78–7.77 (d, 2H, Ar-CH, J = 4 Hz), 7.67–7.63 (t, 1H, imz-CH, J = 8 Hz), 7.50–7.46 (t, 2H, py-CH, Ar-CH, J = 8 Hz), 7.42–7.38 (t, 1H, Ar-CH, J = 8 Hz), 7.04–7.02 (t, 1H, Ar-CH, J = 4 Hz), 6.86–6.84 (t, 1H, imz-CH, J = 8 Hz), 6.60–6.57 (t, 1H, imz-CH, J = 6 Hz); ESI-MS for $C_{18}H_{14}N_3$: 272.11 $[M + H]^+$, found: 272.1182 $[M + H]^+$. Elemental analysis: calculated for $C_{18}H_{13}N_3$: C, 79.68; H, 4.83; N, 15.49%. Found: C, 79.67; H, 4.82; N, 15.48%.

3-(4-Methoxyphenyl)-1-pyridin-2-yl-imidazo[1,5-*a*]pyridine (L2). Ligand L2 was prepared by the reaction of 4-methoxybenzaldehyde (1.25 g, 7.5 mmol), di-pyridin-2-yl-methanone (0.92 g, 5.0 mmol), and NH_4OAc (1.93 g, 25 mmol) upon addition to 25 mL of dry acetic acid. Yellow solid; yield: 62%;

melting range 105–110 °C; ^{1}H NMR (400 MHz, $CDCl_3$) δ 8.72–8.70 (d, 1H, py-CH, J = 8 Hz), 8.65–8.64 (d, 1H, py-CH, J = 4 Hz), 8.27–8.25 (d, 1H, py-CH, J = 8 Hz), 8.2–8.19 (d, 1H, imz-CH, J = 8 Hz), 7.78–7.73 (t, 3H, imz-CH, py-CH, Ar-CH, J = 10 Hz), 7.13–7.07 (m, 3H, Ar-CH, J = 8 Hz), 6.96–6.92 (t, 1H, imz-CH, J = 8 Hz), 6.67–6.64 (t, 1H, imz-CH, J = 6 Hz), 3.9 (s, aryl-OCH_3, 3H); ESI-MS calculated for $C_{19}H_{15}N_3O$: 301.12 (M^+), found: 301.10 (M^+). Elemental analysis: calculated for $C_{19}H_{15}N_3O$: C, 75.73; H, 5.02; N, 13.94%. Found: C, 75.72; H, 5.50; N, 13.91%.

3-(3,4-Dimethoxy-phenyl)-1-pyridin-2-yl-imidazo[1,5-*a*]pyridine (L3). Ligand L3 was prepared by the reaction of 3,4-dimethoxybenzaldehyde (1.25 g, 7.5 mmol), di-pyridin-2-yl-methanone (0.92 g, 5.0 mmol), and NH_4OAc (1.93 g, 25 mmol) upon addition to 25 mL of dry acetic acid. Yellow solid; yield: 68%; melting range, 138–142 °C; ^{1}H NMR (400 MHz, $CDCl_3$) δ 8.72–8.70 (d, 1H, py-CH, J = 8 Hz), 8.65–8.64 (d, 1H, imz-CH, J = 4 Hz), 8.28–8.23 (t, 2H, py-CH, J = 10 Hz), 7.76–7.72 (t, 1H, imz-CH, J = 8 Hz), 7.38–7.35 (d, 2H, Ar-CH, J = 12 Hz), 7.13–7.10 (t, 1H, py-CH, J = 6 Hz), 7.04–7.02 (d, 1H, Ar-CH, J = 8 Hz), 6.96–6.92 (t, 1H, imz-CH, J = 8 Hz), 8.68–8.65 (t, 1H, imz-CH, J = 6 Hz), 3.99–3.97 (d, aryl-OCH_3, 6H, J = 8 Hz); ESI-MS calculated for $C_{20}H_{17}N_3O_2$: 331.13 (M^+), found: 331.11 (M^+). Elemental analysis: calculated for $C_{20}H_{17}N_3O_2$: C, 72.49; H, 5.17; N, 12.68%. Found: C, 72.50; H, 5.16; N, 13.66%.

Dimethyl-[4-(1-pyridin-2-yl-imidazo[1,5-*a*]pyridin-3-yl)phenyl] amine (L4). Ligand L4 was prepared by the reaction of 4-(dimethylamino)benzaldehyde (1.25 g, 7.5 mmol), di-pyridin-2-yl-methanone (0.92 g, 5.0 mmol), and NH_4OAc (1.93 g, 25 mmol) upon addition to 25 mL of dry acetic acid. Yellow solid; yield: 71%; melting range, 176–180 °C; ^{1}H NMR (400 MHz, $CDCl_3$) δ 8.7–8.65 (d, 2H, py-CH, imz-CH, J = 10 Hz), 8.3–8.28 (d, 1H, py-CH, J = 8 Hz), 8.23–8.21 (d, 1H, py-CH, J = 8 Hz), 7.75–7.69 (m, Ar-CH, imz-CH, 3H), 7.12–7.10 (d, 1H, py-CH, J = 8 Hz), 6.93–6.85 (m, imz-CH, Ar-CH, 3H), 6.64–6.61 (t, 1H, imz-CH J = 6 Hz), 3.05 (s, aryl-$N(CH_3)_2$, 6H); ESI-MS calculated for $C_{20}H_{19}N_4$: 315.16 $[M + H]^+$, found: 315.16 $[M + H]^+$. Elemental analysis: calculated for $C_{20}H_{18}N_4$: C, 76.41; H, 5.77; N, 17.82%. Found: C, 76.39; H, 5.75; N, 17.80%.

Synthesis of copper(II) complexes

These complexes were prepared by following the same procedure. An illustrative example is provided below for **1**.

$[Cu(L1)_2(H_2O)](SO_3CF_3)_2$ (1). A acetonitrile (5 mL) solution of $Cu(SO_3CF_3)_2$ of (0.36 g, 1 mmol) was added dropwise to the solution of ligand L1 (0.28 g, 1 mmol) in acetonitrile (5 mL). The solution was stirred at room temperature to obtain a dark-green solution. Suitable single crystals for X-ray analysis were grown by diffusion of diethyl ether. Yield: 0.40 g (63.7%). HR-ESI mass for $[C_{36}H_{26}CuN_6]^{2+}$ (m/z), calculated: 605.15150. Found: 605.15051.

The other complexes, **2–4**, were also synthesized by the method described above under an identical reaction condition.

$[Cu(L2)_2(SO_3CF_3)]SO_3CF_3$ (2). Yield: 0.39 g (60%). HR-ESI mass for $[C_{39}H_{30}CuF_3N_6O_5S]^+$ (m/z), calculated: 814.12465; found: 814.12347.

$[Cu(L3)_2(H_2O)](SO_3CF_3)_2$ (3). Yield: 0.47 g (70%). HR-ESI mass for $[C_{40}H_{34}CuN_6O_4]^{2+}$ (m/z), calculated: 725.28176; found: 725.19281.

$[Cu(L4)_2(H_2O)](SO_3CF_3)_2$ (4). Yield: 0.38 g (58%). HR-MS mass for $[C_{40}H_{36}CuN_8]^{2+}$ (m/z), calculated: 691.23589; found: 691.23590.

Characterization of $[Cu(L2)_2(Cys)]$. ^{1}H NMR (400 MHz, DMSO and D_2O mixture) δ 8.49–8.48 (d, 1H, J = 4.5 Hz, CH_{Ar}), 8.39–8.37 (d, 1H, J = 6.7 Hz, CH_{Ar}), 8.24–8.22 (d, 1H, J = 9.1 Hz, CH_{Ar}), 8.15 (dd, 2H, J = 15.5, 7.6 Hz, CH_{Ar}), 7.74–7.72 (2, 2H, J = 7.4 Hz, CH_{Ar}), 7.41 (s, 1H, CH_{Ar}), 7.24–7.17 (m, 1H, CH_{Ar}), 7.13–7.11 (d, 2H, J = 7.5 Hz, CH_{Ar}), 6.92–6.88 (t, 1H, J = 6.5 Hz, CH_{Ar}). 3.79 (S, 4H, OCH_3, α-CH), 2.91(s, 2H, β-CH_2). HR-MS, m/z, 785.3256 (calculated for 785.18455). FT-IR stretching frequencies ($\bar{\nu}$) 2915, 1577, 1482 and 1401 cm^{-1} and were well-shifted from free Cys and matched with $\bar{\nu}_{st}$ of Cu^I-(Cys). Elemental analysis: calculated for $CuC_{41}H_{36}N_7O_4S$: C, 62.62; H, 4.61; N, 12.47. Found as C, 62.60; H, 4.60; N, 12.44.

Conflicts of interest

The authors declare no conflicts of interest.

Acknowledgements

We acknowledge the Science and Engineering Research Board (SERB), New Delhi, Board of Research in Nuclear Sciences (BRNS), Mumbai and Department of Biotechnology (DBT), New Delhi, India for funding.

References

1 (*a*) C. Hwang, A. J. Sinskey and H. F. Lodish, *Science*, 1992, **257**, 1496–1502; (*b*) J. B. Schulz, J. Lindenau, J. Seyfried and J. Dichgans, *Eur. J. Biochem.*, 2000, **267**, 4904–4911; (*c*) S. Seshadri, A. Beiser, J. Selhub, P. F. Jacques, I. H. Rosenberg, R. B. D'Agostino, P. W. F. Wilson and P. A. Wolf, *N. Engl. J. Med.*, 2002, **346**, 476–483; (*d*) Z. A. Wood, E. Schroder, J. R. Harris and L. B. Poole, *Trends Biochem. Sci.*, 2003, **28**, 32–40; (*e*) H. Refsum, A. D. Smith, P. M. Ueland, E. Nexo, R. Clarke, J. McPartlin, C. Johnston, F. Engbaek, J. Schneede, C. McPartlin and J. M. Scott, *Clin. Chem.*, 2004, **50**, 3–32; (*f*) R. Hong, G. Han, J. M. Fernandez, B.-j. Kim, N. S. Forbes and V. M, *J. Am. Chem. Soc.*, 2006, **128**, 1078–1079.

2 R. K. Pathak, V. K. Hinge, K. Mahesh, A. Rai, D. Panda and C. P. Rao, *Anal. Chem.*, 2012, **84**, 6907–6913.

3 R. K. Pathak, K. Tabbasum, A. Rai, D. Panda and C. P. Rao, *Analyst*, 2012, **137**, 4069–4075.

4 R. Peng, L. Lin, X. Wu, X. Liu and X. Feng, *J. Org. Chem.*, 2013, **78**, 11602–11605.

5 G. Reddy, H. Agarwalla, N. Taye, S. Ghorai, S. Chattopadhyay and A. Das, *Chem. Commun.*, 2014, **50**, 9899–9902.
6 S.-Q. Wang, Q.-H. Wu, H.-Y. Wang, X.-X. Zheng, S.-L. Shen, Y.-R. Zhang, J.-Y. Miao and B.-X. Zhao, *Analyst*, 2013, **138**, 7169–7174.
7 C. Yin, F. Huo, J. Zhang, R. Martinez-Manez, Y. Yang, H. Lv and S. Li, *Chem. Soc. Rev.*, 2013, **42**, 6032–6059.
8 L.-Y. Niu, Y.-S. Guan, Y.-Z. Chen, L.-Z. Wu, C.-H. Tung and Q.-Z. Yang, *Chem. Commun.*, 2013, **49**, 1294–1296.
9 W. Hao, A. McBride, S. McBride, J. P. Gao and Z. Y. Wang, *J. Mater. Chem.*, 2011, **21**, 1040–1048.
10 F. Kong, R. Liu, R. Chu, X. Wang, K. Xu and B. Tang, *Chem. Commun.*, 2013, **49**, 9176–9178.
11 D. Maheshwaran, S. Priyanga and R. Mayilmurugan, *Dalton Trans.*, 2017, **46**, 11408–11417.
12 (*a*) V. Turk, J. Kos and B. Turk, *Cancer Cell*, 2004, **5**, 409–410; (*b*) J. A. Joyce and D. Hanahan, *Cell Cycle*, 2004, **3**, 1516–1519; (*c*) M. M. Mohamed and B. F. Sloane, *Nat. Rev. Cancer*, 2006, **6**, 764–775; (*d*) S. P. Fricker, *Metallomics*, 2010, **2**, 366–377; (*e*) V. Turk, V. Stoka, O. Vasiljeva, M. Renko, T. Sun, B. Turk and D. Turk, *Biochim. Biophys. Acta*, 2012, **1824**, 68–88; (*f*) G. J. Tan, Z. K. Peng, J. P. Lu and F. Q. Tang, *World J. Biol. Chem.*, 2013, **4**, 91–101.
13 L. Klein, M. Hinterberger, G. Wirnsberger and B. Kyewski, *Nat. Rev. Immunol.*, 2009, **9**, 833–844.
14 Z. Mao, M. Wang, J. Liu, L.-J. Liu, S. M.-Y. Lee, C.-H. Leung and D.-L. A. Ma, *Chem. Commun.*, 2016, **52**, 4450–4453.
15 Q. Lin, Y. Huang, J. Fan, R. Wang and N. Fu, *Talanta*, 2013, **114**, 66–72.
16 X. Li, S. Qian, Q. He, B. Yang, J. Li and Y. Hu, *Org. Biomol. Chem.*, 2010, **8**, 3627–3630.
17 L. Yuan, W. Lin, S. Zhao, W. Gao, B. Chen, L. He and S. Zhu, *J. Am. Chem. Soc.*, 2012, **134**, 13510–13523.
18 A. Y. Cho and K. Choi, *Chem. Lett.*, 2012, **41**, 1611–1612.
19 L.-Y. Niu, H.-R. Zheng, Y.-Z. Chen, L.-Z. Wu, C.-H. Tung and Q.-Z. Yang, *Analyst*, 2014, **139**, 1389–1395.
20 C. Ge, H. Wang, B. Zhang, J. Yao, X. Li, W. Feng, P. Zhou, Y. Wang and J. Fang, *Chem. Commun.*, 2015, **51**, 14913–14916.
21 (*a*) T. Ma, H. Ding, H. Xu, Y. Lv, H. Liu, H. Wang and Z. Tian, *Analyst*, 2015, **140**, 322–329; (*b*) J. Zhang, J. Wang, J. Liu, L. Ning, X. Zhu, B. Yu, X. Liu, X. Yao and H. Zhang, *Anal. Chem.*, 2015, **87**, 4856–4863; (*c*) Q. Miao, Q. Li, Q. Yuan, L. Li, Z. Hai, S. Liu and G. Liang, *Anal. Chem.*, 2015, **87**, 3460–3466; (*d*) Y. Hu, C. H. Heo, G. Kim, E. J. Jun, J. Yin, H. M. Kim and J. Yoon, *Anal. Chem.*, 2015, **87**, 3308–3313; (*e*) M.-Y. Jia, L.-Y. Niu, Y. Zhang, Q.-Z. Yang, C.-H. Tung, Y.-F. Guan and L. Feng, *ACS Appl. Mater. Interfaces*, 2015, **7**, 5907–5914; (*f*) D. Zhang, Z. Yang, H. Li, Z. Pei, S. Sun and Y. Xu, *Chem. Commun.*, 2016, **52**, 749–752.
22 (*a*) L.-Y. Niu, Y.-S. Guan, Y.-Z. Chen, L.-Z. Wu, C.-H. Tung and Q.-Z. Yang, *J. Am. Chem. Soc.*, 2012, **134**, 18928–18931; (*b*) F. Wang, Z. Guo, X. Li, X. Li and C. Zhao, *Chem. – Eur. J.*, 2014, **20**, 11471–11478; (*c*) J. Yin, Y. Kwon, D. Kim, D. Lee, G. Kim, Y. Hu, J.-H. Ryu and J. Yoon, *J. Am. Chem. Soc.*, 2014, **136**, 5351–5358; (*d*) F. Wang, L. Zhou, C. Zhao, R. Wang, Q. Fei, S. Luo, Z. Guo, H. Tian and W.-H. Zhu, *Chem. Sci.*, 2015, **6**, 2584–2589.
23 (*a*) Y. G. Shi, J. H. Yao, Y. L. Duan, Q. L. Mi, J. H. Chen, Q. Q. Xu, G. Z. Gou, Y. Zhou and J. F. Zhang, *Bioorg. Med. Chem. Lett.*, 2013, **23**, 2538–2542; (*b*) C.-C. Zhao, Y. Chen, H.-Y. Zhang, B.-J. Zhou, X.-J. Lv and W.-F. Fu, *J. Photochem. Photobiol., A*, 2014, **282**, 41–46.
24 (*a*) A. Loas, R. J. Radford, A. D. Liang and S. J. Lippard, *Chem. Sci.*, 2015, **6**, 4131–4140; (*b*) J. A. Cotruvo Jr., A. T. Aron, K. M. Ramos-Torresa and C. J. Chang, *Chem. Soc. Rev.*, 2015, **44**, 4400–4414; (*c*) L. E. McQuade and S. J. Lippard, *Curr. Opin. Chem. Biol.*, 2010, **14**, 43–49; (*d*) U.-P. Apfel, D. Buccella, J. J. Wilson and S. J. Lippard, *Inorg. Chem.*, 2013, **52**, 3285–3294; (*e*) A. T. Wrobel, T. C. Johnstone, A. D. Liang, S. J. Lippard and P. Rivera-Fuentes, *J. Am. Chem. Soc.*, 2014, **136**, 4697–4705; (*f*) S. Kim, M. A. Minier, A. Loas, S. Becker, F. Wang and S. J. Lippard, *J. Am. Chem. Soc.*, 2016, **138**, 1804–1807; (*g*) A. Loas and S. J. Lippard, *J. Mater. Chem. B*, 2017, **5**, 8929–8933; (*h*) M. D. Pluth, L. E. McQuade and S. J. Lippard, *Org. Lett.*, 2010, **12**, 2318–2321.
25 (*a*) W. E. Blumberg, *J. Chem. Phys.*, 1968, **49**, 1793–1802; (*b*) I. M. Klotzg, G. H. Czerlinski and H. A. FIESS, *J. Am. Chem. Soc.*, 1958, **80**, 2920–2923; (*c*) H. K. Baek, R. L. Cooper and R. A. Holwerda, *Inorg. Chem.*, 1985, **24**, 1077–1081.
26 A. Rigo, A. Corazza, M. L. D. Paolo, M. Rossetto, R. Ugolini and M. Scarpa, *J. Inorg. Biochem.*, 2004, **98**, 1495–1501.
27 D. Maheshwaran, T. Nagendraraj, P. Manimaran, B. Ashokkumar, M. Kumar and R. Mayilmurugan, *Eur. J. Inorg. Chem.*, 2017, **2017**, 1007–1016.
28 (*a*) A. Rahmathi and Z. Khalesi, *Int. J. Org. Chem.*, 2011, **1**, 15–19; (*b*) J. Wang, L. Dyers, R. Mason, P. Amoyaw and X. R. Bu, *J. Org. Chem.*, 2005, **70**, 2353–2356.
29 A. W. Addison and T. N. Rao, *J. Chem. Soc., Dalton Trans.*, 1984, 1349.
30 (*a*) C. H. Kjaergaard, S. M. Jones, S. Gounel, N. Mano and E. I. Solomon, *J. Am. Chem. Soc.*, 2015, **137**, 8783–8794; (*b*) E. I. Solomon, *Inorg. Chem.*, 2016, **55**, 6364–6375; (*c*) M. J. Bew, B. J. Hathaway and R. J. Fereday, *J. Chem. Soc., Dalton Trans.*, 1972, 1229; (*d*) E. Selimović, A. V. Komolkin, A. V. Egorov and T. Soldatović, *J. Coord. Chem.*, 2018, **71**, 1003–1019.
31 E. I. Solomon, D. E. Heppner, E. M. Johnston, J. W. Ginsbach, J. Cirera and M. Qayyum, *Chem. Rev.*, 2014, **114**, 3659–3853.
32 M. Murali, M. Palaniandavar and T. Pandiyan, *Inorg. Chim. Acta*, 1994, **224**, 19–25.
33 (*a*) C. Rajarajeswari, R. Loganathan, M. Palaniandavar, E. Suresh, A. Riyasdeen and M. A. Akbarsha, *Dalton Trans.*, 2013, **42**, 8347–8363; (*b*) S. Gupta and M. K. Maheshwari, *Chem. Sci. Trans.*, 2013, **2**, 927–935.
34 S. Muthuramalingam, T. Khamrang, M. Velusamy and R. Mayilmurugan, *Dalton Trans.*, 2017, **46**, 16065–16076.

35 I. M. Kooter, R. A. Steiner, B. W. Dijkstra, P. I. Van Noort, M. R. Egmond and M. Huber, *Eur. J. Biochem.*, 2002, **269**, 2971–2979.
36 (*a*) J. S. Hyde and W. Froncisz, *Annu. Rev. Biophys. Bioeng.*, 1982, **11**, 391–417; (*b*) J. L. Cole, G. O. Tan, E. K. Yang, K. O. Hodgson and E. I. Solomon, *J. Am. Chem. Soc.*, 1990, **112**, 2243–2249.
37 E. I. Solomon, R. K. Szilagyi, S. D. George and L. Basumallick, *Chem. Rev.*, 2004, **104**, 419–458.
38 P. Jaividhya, M. Ganeshpandian, R. Dhivya, M. A. Akbarsha and M. Palaniandavar, *Dalton Trans.*, 2015, **44**, 11997–12010.
39 E. I. Solomon, *Inorg. Chem.*, 2006, **45**, 8012–8025.
40 (*a*) B. J. Hathaway, G. Wilkinson, R. D. Gillard and J. A. McCleverty, *Comprehensive Coordination Chemistry*, Pergamon, Oxford, 1987, vol. 5; (*b*) P. F. Rapheal, E. Manoj and M. R. P. Kurup, *Polyhedron*, 2007, **26**, 818–828.
41 A. Rockenbauer, *J. Magn. Reson.*, 1979, **35**, 429–438.
42 (*a*) M. Assour, *J. Chem. Phys.*, 1965, **43**, 2477; (*b*) A. Abragam and M. H. L. Pryce, *Proc. R. Soc. London, Ser. A*, 1961, **206**, 164.
43 (*a*) B. J. Hathaway, *J. Chem. Soc., Dalton Trans.*, 1972, 1196; (*b*) M. Duggan, N. Ray, B. Hathaway, G. Tomlinson, P. Brint and K. Pelin, *J. Chem. Soc., Dalton Trans.*, 1980, 1342–1348.
44 (*a*) B. J. Hathaway and D. E. Billing, *Coord. Chem. Rev.*, 1970, **5**, 143–207; (*b*) B. J. Hathaway and A. A. G. Tomlinson, *Coord. Chem. Rev.*, 1970, **5**, 143.
45 A. Rigo, A. Corazza, M. L. D. Paolo, M. Rossetto, R. Ugolini and M. Scarpa, *J. Inorg. Biochem.*, 2004, **98**, 1495–1501.
46 K. M. Dokken, J. G. Parsons, J. McClure and J. L. Gardea-Torresdey, *Inorg. Chim. Acta*, 2009, **362**, 395–401.
47 B. K. Maiti, L. B. Maia, A. J. Moro, J. C. Lima, C. M. Cordas, I. Moura and J. J. G. Moura, *Inorg. Chem.*, 2018, **57**, 8078.
48 P. B. Tsitovich, P. J. Burns, A. M. McKay and J. R. Morrow, *J. Inorg. Biochem.*, 2014, **133**, 143–154.
49 Y. Ke, J. Zhao, U. H. Verkerk, A. C. Hopkinson and K. W. M. Siu, *J. Phys. Chem. B*, 2007, **111**, 14318–14328.
50 R. K. Singh, S. K. Verma and P. D. Sharma, *Int. J. ChemTech Res.*, 2011, **3**, 1571.
51 R. K. Pathak, V. K. Hinge, K. Mahesh, A. Rai, D. Panda and C. P. Rao, *Anal. Chem.*, 2012, **84**, 6907–6913.
52 Z. Huang, J. Du, J. Zhang, X. Q. Yu and L. Pu, *Chem. Commun.*, 2012, **48**, 3412–3414.
53 (*a*) S. G. Tajc, B. S. Tolbert, R. Basavappa and B. L. Miller, *J. Am. Chem. Soc.*, 2004, **126**, 10508–10509; (*b*) A. V. Glushchenko and D. W. Jacobsen, *Antioxid. Redox Signaling*, 2007, **9**, 1883–1898.
54 K. L. Haas and K. J. Franz, *Chem. Rev.*, 2009, **109**, 4921–4960.
55 J. Cheng, X. Zhou and H. Xiang, *Analyst*, 2015, **140**, 7082–7115.
56 (*a*) D. B. Rorabacher, *Chem. Rev.*, 2004, **104**, 651–697; (*b*) E. I. Solomon, D. E. Heppner, E. M. Johnston, J. W. Ginsbach, J. Cirera, M. Qayyum, M. T. Kieber-Emmons, C. H. Kjaergaard, R. G. Hadt and L. Tian, *Chem. Rev.*, 2014, **114**, 3659–3853; (*c*) K. Tsuge, F. DeRosa, M. D. Lim and P. C. Ford, *J. Am. Chem. Soc.*, 2004, **126**, 6564–6565; (*d*) S. Kim, M. A. Minier, A. Loas, S. Becker, F. Wang and S. J. Lippard, *J. Am. Chem. Soc.*, 2016, **138**, 1804–1807.
57 (*a*) D. M. Arciero, B. S. Pierce, M. P. Hendrich and A. B. Hooper, *Biochemistry*, 2002, **41**, 1703–1709; (*b*) K. N. Chacon and N. J. Blackburn, *J. Am. Chem. Soc.*, 2012, **134**, 16401–16412; (*c*) L. Basumallick, R. Sarangi, S. D. George, B. Elmore, A. B. Hooper, B. Hedman, K. O. Hodgson and E. I. Solomon, *J. Am. Chem. Soc.*, 2005, **127**, 3531–3544; (*d*) G. J. Kavarnos and N. Turro, *J. Chem. Rev.*, 1986, **86**, 401–449.
58 A. E. Palmer, D. W. Randall, F. Xu and E. I. Solomon, *J. Am. Chem. Soc.*, 1999, **121**, 7138–7149.
59 M. J. Frisch, G. W. Trucks, H. B. Schlegel, G. E. Scuseria, M. A. Robb, J. R. Cheeseman, G. Scalmani, V. Barone, B. Mennucci, G. A. Petersson, H. Nakatsuji, M. Caricato, X. Li, H. P. Hratchian, A. F. Izmaylov, J. Bloino, G. Zheng, J. L. Sonnenberg, M. Hada, M. Ehara, K. Toyota, R. Fukuda, J. Hasegawa, M. Ishida, T. Nakajima, Y. Honda, O. Kitao, H. Nakai, T. Vreven, J. A. Montgomery Jr., J. E. Peralta, F. Ogliaro, M. J. Bearpark, J. Heyd, E. N. Brothers, K. N. Kudin, V. N. Staroverov, R. Kobayashi, J. Normand, K. Raghavachari, A. P. Rendell, J. C. Burant, S. S. Iyengar, J. Tomasi, M. Cossi, N. Rega, N. J. Millam, M. Klene, J. E. Knox, J. B. Cross, V. Bakken, C. Adamo, J. Jaramillo, R. Gomperts, R. E. Stratmann, O. Yazyev, A. J. Austin, R. Cammi, C. Pomelli, J. W. Ochterski, R. L. Martin, K. Morokuma, V. G. Zakrzewski, G. A. Voth, P. Salvador, J. J. Dannenberg, S. Dapprich, A. D. Daniels, Ö. Farkas, J. B. Foresman, J. V. Ortiz, J. Cioslowski and D. J. Fox, *Gaussian 09*, 2009.